Hindawi
International Journal of RF and Microwave Computer-Aided Engineering
Volume 2023, Article ID 9533725, 14 pages
https://doi.org/10.1155/2023/9533725

Research Article

A High-Frequency Planar-Configured Millimeter-Wave MIMO Antenna for Fifth-Generation NR Operations

Poonam Tiwari,[1] **Vishant Gahlaut**,[1] **Meenu Kaushik**,[2] **Anshuman Shastri**,[3] **Gulman Siddiqui**,[1] **and Bhupender Singh**[4]

[1]*Department of Physical Sciences, Banasthali Vidyapith, Rajasthan, India*
[2]*School of Automation, Banasthali Vidyapith, Rajasthan, India*
[3]*Centre for Artificial Intelligence, Banasthali Vidyapith, Rajasthan, India*
[4]*Department of Water Supply and Environmental Engineering, Arba Minch University, Arba Minch, Ethiopia*

Correspondence should be addressed to Bhupender Singh; bhupender.sandher@amu.edu.et

Received 10 June 2023; Revised 9 September 2023; Accepted 16 September 2023; Published 30 September 2023

Academic Editor: Giacomo Muntoni

This article presents a simple planar millimeter-wave (mm-wave) multiple input multiple output (MIMO) antenna with four closely spaced radiating elements. The antenna is intended to enhance the bandwidth for 5G new radio (NR) applications and also cover the industrial Ka-band (26.5-40 GHz), Q-band (30-50 GHz), and U-band (40-60 GHz) frequency ranges. The antenna is designed using Rogers RT/duroid 5880 substrate with a size of $25 \times 26 \times 1.6\,\text{mm}^3$. The proposed antenna consists of four identical radiating elements with two of them positioned in a linear configuration facing each other, while the other two elements are placed opposite to the first two, which improves isolation between the elements. Across the entire operating frequency range (26-60 GHz), the antenna demonstrated excellent performance, including 34 GHz wide bandwidth, high isolation of >25 dB, nearly omnidirectional radiation patterns, high gain of 11.1 dB with a high radiation efficiency of 94%, low envelope correlation coefficient (ECC) of 0.0068, and high diversity gain (DG) of 9.967 dB. The simulated findings exhibit a strong positive correlation with the experimental results. The proposed MIMO antenna design is a promising solution for 5G NR applications.

1. Introduction

The utilization of mm-wave band technology has become an essential aspect of the fifth-generation (5G) systems. With the growing demand for faster data rates, increased traffic congestion, and the need for more efficient appliances, researchers are focused on developing 5G communication systems that meet these requirements [1]. The mm-wave frequency bands are utilized in 5G range from 24 to 100 GHz, which enables seamless communication across various technologies, including smart homes, telemedicine, virtual reality, and the Internet of Vehicles (IoV) [2].

To support these applications, mm-wave antennas must be wideband, cost-effective, elevated, and capable of designing and manufacturing. In 5G NR, two frequency bands are recognized: frequency range 1 (FR1) and frequency range 2 (FR2). The FR1 ranges from 410 to 7125 MHz and primarily utilizes sub-6 GHz frequencies previously used by fourth-generation/long-term evolution (4G/LTE) networks. However, these frequencies are not sufficient to support groundbreaking advancements in the 5G NR nonstandalone architecture, although they can still significantly enhance 5G networks. On the other hand, FR2, also known as the mm-wave range, operates between 24.25 GHz and 52.6 GHz, as depicted in Figure 1. This frequency range provides the necessary support for the advanced features of 5G systems, making it crucial to the success of 5G communication technology. The use of mm-wave frequencies in 5G wireless networks provides numerous benefits for customers, businesses, and network operators due to its wider frequency bandwidth and higher channel capacity [3]. However, the properties of mm-waves make the planning of networks that

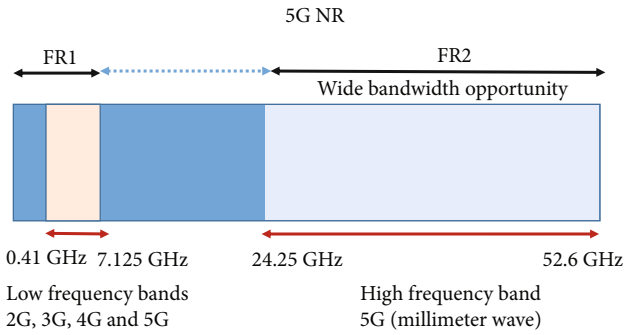

Figure 1: 5G NR frequency ranges.

use these frequencies significantly more difficult [4]. To standardize 5G wireless communication networks, regulators, telecoms sector, and governments are putting in a lot of effort, with the 26 GHz and 28 GHz bands being considered for 5G communications by most countries [5, 6]. To meet the increasing demand for low-cost, low-power, and high data rate requirements, the mm-wave band is considered to play a vital role in 5G wireless networks [7]. Horn antennas are suitable for this purpose due to their wide bandwidth and gain, but their bulky design and complex feed area make them challenging to use in array applications and integrate with planar circuits [8].

In 5G communication, high-gain antennas are crucial due to increasing atmospheric and propagation losses at mm-wave bands. However, traditional high-gain approaches suffer from drawbacks such as large profiles, complex geometries, nonplanar structures, and bulky volumes [9]. To overcome these challenges, advanced techniques like MIMO technology have been developed, offering improved signal coverage, anti-interference capabilities, and high gain. Several methods, such as super state over patch antennas, stacked patch substrates, lens-coupled antennas, and dielectric resonator antennas (DRAs), have been utilized to enhance antenna gain. Additionally, antenna arrays are a widely recognized method for achieving high gain [10–17].

This paper proposes an mm-wave MIMO antenna that overcomes the challenges and limitations of the previous investigations. The antenna design is simple and planar and exhibits wide bandwidth, making it suitable for 5G NR applications. The overall proposed design of the MIMO antenna is quite original in its approach; it includes a relatively simpler design that produces excellent output on various parameters such as high gain, wide bandwidth, and good efficiency. In comparison to a single antenna, these features can be improved by implementing MIMO design. Also, we have designed the antenna without using any decoupling or extra structure, and it is self-isolated within the operating band. This unique combination sets the proposed antenna apart from the previous studies, where frequency ranges and performance metrics differ considerably. The novel MIMO configuration contributes to its novelty and potential for various high-frequency applications. The significance of such a design lies in its ability to achieve specific performance goals.

The paper is structured into six sections, beginning with an introduction that outlines the research objectives. Section 2 describes the geometric design evolutions of a single-antenna element, followed by Section 3, which presents the extension of the design to two antenna elements. In Section 4, the proposed four-antenna element with a fabricated structure is presented. The results and discussions of the proposed antenna are demonstrated in Section 5, and finally, the paper concludes with a summary of the findings in Section 6.

2. Antenna Design Methodology

The antenna design process involved three iterative steps, with each step featuring different antenna configurations. Starting with a single-element antenna ($16 \times 10 \times 1.6\,\text{mm}^3$), it progressed to a two-element MIMO antenna ($20 \times 18 \times 1.6\,\text{mm}^3$) and finally to a four-element MIMO antenna ($25 \times 26 \times 1.6\,\text{mm}^3$). The substrate used was Rogers RT/duroid 5880, featuring a thickness of 1.6 mm, a relative permittivity (ε_r) of 2.2, and a low loss tangent (tan δ) of 0.0009. The full ground plane for each step is same as the dimension of substrate. A 50 Ω microstrip transmission line fed each antenna element. Simulations were performed to optimize the design and achieve the desired performance metrics.

2.1. Single-Antenna Configuration—First Iteration. The parameters for a single antenna are optimized in the context of wideband performance through four steps as depicted in Figure 2(a).

Step 1. The process begins with a rectangular printed antenna featuring a microstrip transmission line on a simple rectangular patch with a full ground plane. However, this initial antenna has poor impedance matching and a narrow bandwidth.

To address these issues:

Step 2. The corner of the rectangular patch is cut to introduce deliberate wave propagation discontinuities, increasing reflection and enhancing the impedance bandwidth.

Step 3. A rectangular stub ($8 \times 5\,\text{mm}^2$) is added next to the transmission line and involves a complex interplay of electromagnetic effects to further widen the impedance bandwidth without changing the antenna's size.

Step 4. A rectangular slot ($6.8 \times 0.5\,\text{mm}^2$) is integrated into the rectangular stub with a full ground layer. This optimizes the current path, resulting in a significantly broader impedance bandwidth with multiple frequency bands. The final result is a perfect fractal structure (Figure 2(b)) with improved impedance matching and a wide bandwidth, suitable for various practical applications.

The design modifications that followed have resulted in significant improvements in various characteristics of the system, including a wider bandwidth, lower reflection

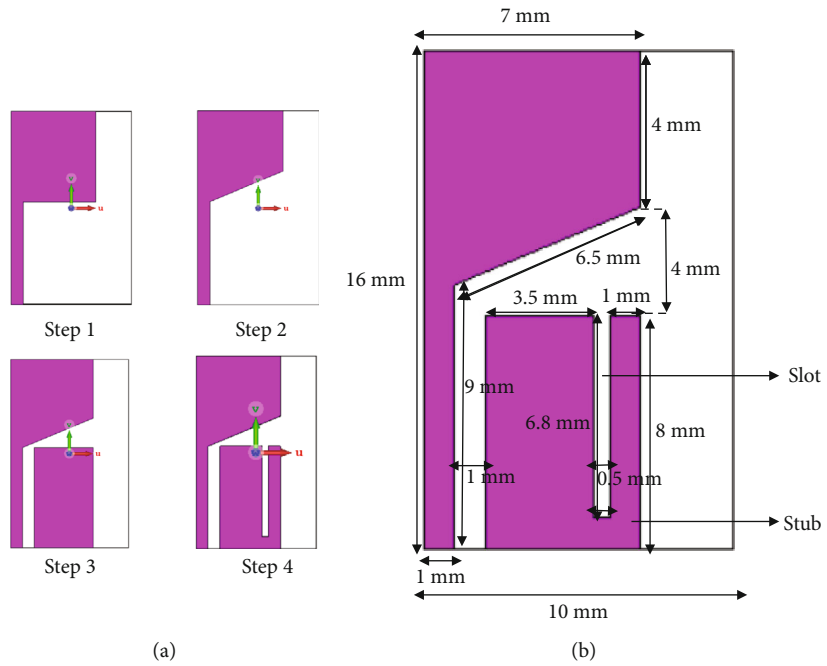

FIGURE 2: (a) Design progression of single-element antenna. (b) Single-element antenna configuration with parametric values.

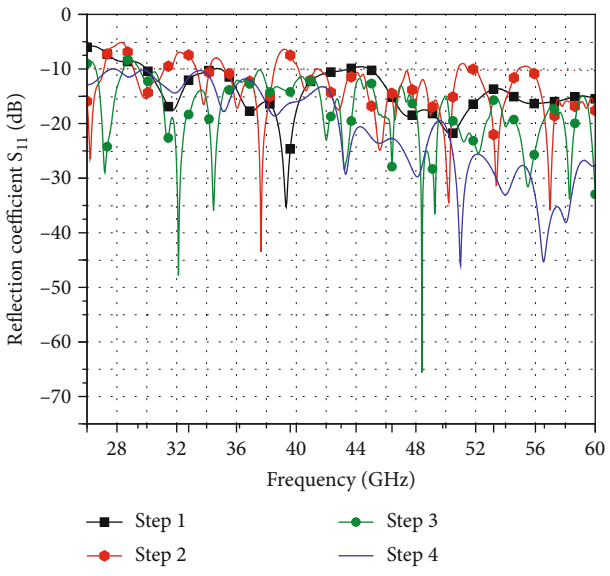

FIGURE 3: Simulated reflection coefficient ($|S_{11}|$) in all four steps for single-element antenna.

coefficient, and higher radiation efficiency. The optimized values of the design parameters for this configuration, without any changes to the ground, are shown in detail in Figure 2(b).

Figure 3 displays a comparison of reflection coefficients $|S_{11}|$ for all four fractal steps of an antenna design. In Step 1, the antenna exhibited a triple-band response in the frequency range of 29.9-34.4 GHz, 34.9-43.5 GHz, and 44.5-60 GHz, with resonant frequencies of 31.6 GHz, 39.2 GHz, and 50.1 GHz due to the high impedance matching over these frequency bands. Subsequently, in Step 2, the antenna generated multiple frequency bands, including 26-27.1 GHz, 29.1-31.2 GHz, 33.3-34.1 GHz, 35.2-38.5 GHz, 40.1-40.9 GHz, 41-54.8 GHz, and 55.7-60 GHz, with resonant frequencies of 26.2 GHz, 29.9 GHz, 34 GHz, 37.6 GHz, 40.6 GHz, 45.6 GHz, and 57.1 GHz showing better impedance matching in these resonant frequencies. In Step 3, the antenna generated dual-band responses from 26.5 to 28.4 GHz and 29.5 to 60 GHz, with resonant frequencies of 27.1 GHz and 48.4 GHz, respectively. Finally, in Step 4, the antenna achieved good impedance matching between the patch and transmission line with stub and slot, resulting in $|S_{11}| < -10$ dB and voltage standing wave ratio (VSWR < 2) with a wideband characteristic across the entire operating frequency range of 26-60 GHz. The simulated results for single-element antennas demonstrated that a bandwidth of 34 GHz was achieved over the entire frequency range of 26-60 GHz. Overall, the results indicate that as the fractal steps increase, the antenna design achieves better impedance matching and wider bandwidth.

The surface current distribution at the center frequency of 43 GHz for all four design steps is presented in Figures 4(a)–4(d), allowing for a better understanding of the antenna's working mechanism.

In Step 1, the current is mostly dispersed near the feed line and at the lower side edge of the patch antenna (Figure 4(a)). This concentration of current is indicative resonant behavior of the antenna. The geometry of the patch and feed line at this stage leads to resonance within the frequency band. When the corner of the rectangular patch is cut, a significant amount of current is integrated near the patch's edge (Figure 4(b)). The disruption in the current flow path can lead to a shift in the resonant frequency of antenna. In this case, it likely contributes to the ability of

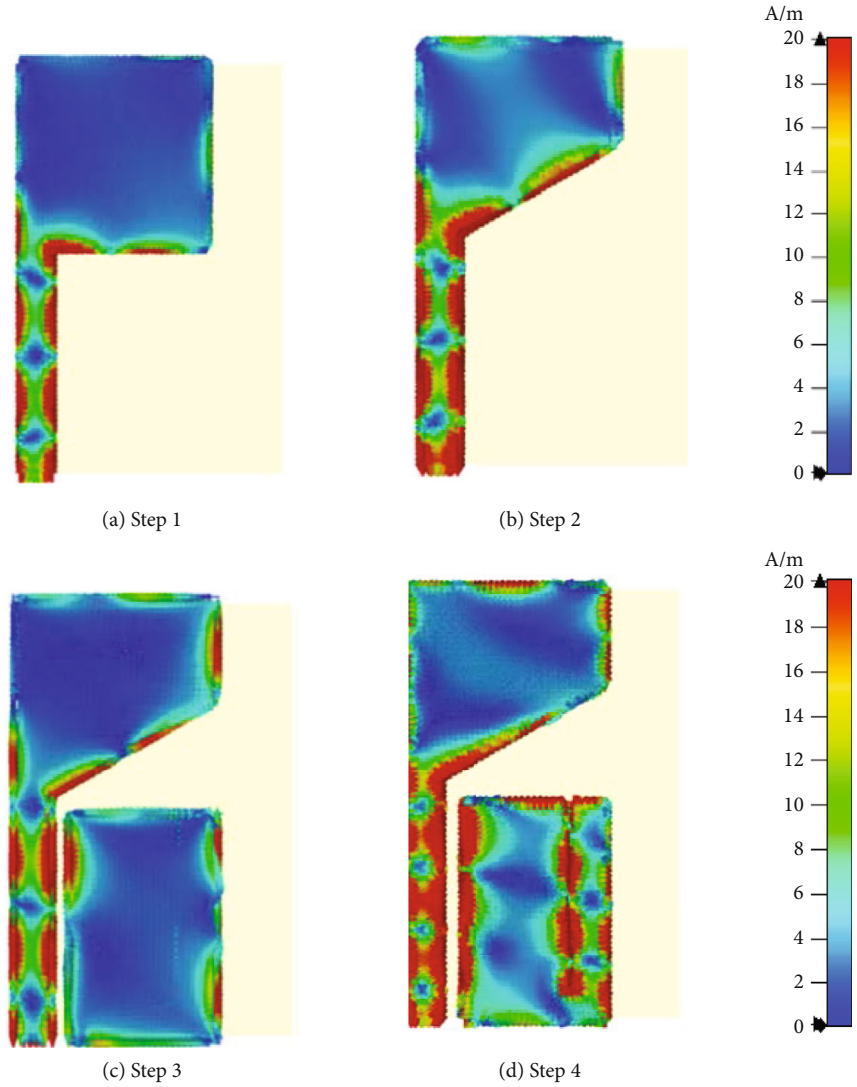

FIGURE 4: Surface current distribution at center frequency of 43 GHz for each step of the single-element antenna.

the antenna to resonate at higher frequencies within the specified band. The addition of a rectangular stub to the patch antenna increases the current flow at the edges of the antenna, with some current also observed at the edges of the stub later (Figure 4(c)). This modification increases the current flow at the edges of the antenna, which can lead to an expansion of the antenna's bandwidth. It contributes to the ability of antenna to resonate at higher frequencies. The placement of the slot on the rectangular stub alters the current path, thereby increasing the path length (Figure 4(d)). As a result, the current density is observed at the radiating patch with feed around the rectangular stub with a slot. Consequently, the resonant band has significantly shifted towards the wideband, achieving the desired frequency range, as shown in Figure 4. Therefore, the surface current density provides a visual representation of how cutting the corner, adding the stub, and etching the slot contributed to achieving the desired bandwidth.

Figure 5(a) illustrates the optimization process for adjusting the position of a rectangular slot (referred to as Rs) at four distinct locations (Rs1 to Rs4). This deliberate adjustment of Rs position serves as a means to achieve resonance at multiple frequencies. The antenna is tuned to radiate or receive electromagnetic waves at several different frequencies efficiently. To put it more simply, Figure 5(b) demonstrates how changing the placement of Rs1 to Rs4 allows the antenna to work effectively by $|S_{11}|$ at wideband with multiple resonant frequencies. The rectangular slot on the stub can introduce additional coupling mechanisms and resonance modes. The dimensions and location of the slot play a crucial role in determining the resonance frequencies with wideband operation of the antenna.

3. Two-Element MIMO Antenna Configuration—Second Iteration

The antenna design has been upgraded from a single-element to a two-element MIMO antenna (Figure 6). The two microstrip antennas are symmetrically placed on a substrate measuring $16 \times 18\,\text{mm}^2$. The dimensions of a patch antenna and a

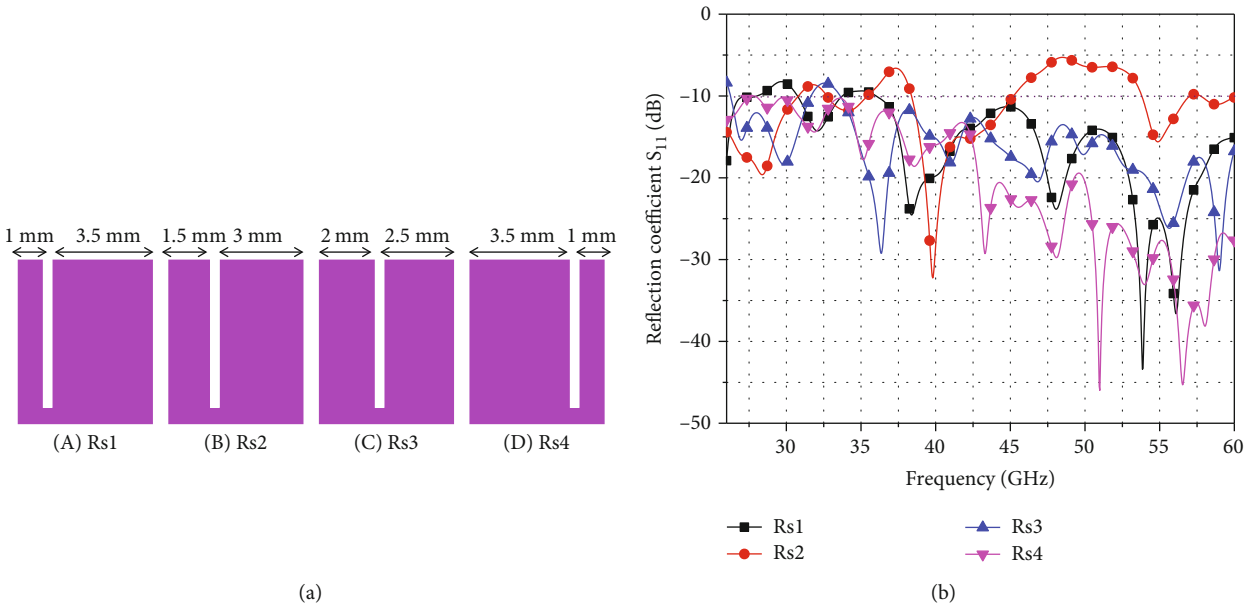

FIGURE 5: (a) Optimization of rectangular slot (Rs) at different positions. (b) Optimized reflection coefficient ($|S_{11}|$) for rectangular slot (Rs) at different positions.

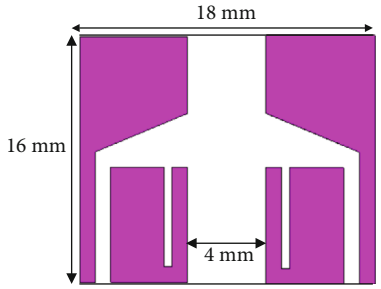

FIGURE 6: Two-element MIMO antenna geometry.

transmission line are comparable to those of a single-antenna element. The modification resulted in improved bandwidth, higher isolation, and increased signal strength compared to the previous design. This can result in better overall system performance and improved signal-to-noise ratio, reduce interference, and improve overall system reliability.

The results of a simulation for a two-element MIMO antenna are presented in Figure 7, displaying the plots of reflection coefficient $|S_{11}|$ and $|S_{22}|$ and transmission coefficient $|S_{12}|$ and $|S_{21}|$. It is evident from the graph that $|S_{11}|$ and $|S_{22}|$ behave similarly, so as $|S_{12}|$ and $|S_{21}|$. The bandwidth covers the frequency range of 26-60 GHz, with $|S_{11}|$ showing values less than -10 dB (VSWR ≤ 2) reaching up to 60 GHz. The minimum magnitude of $|S_{11}|$ is -63 dB, which occurs at 56.2 GHz. Furthermore, the simulated $|S_{12}|$ and $|S_{21}|$ are less than -20 dB across the entire frequency range, indicating low mutual coupling between the antenna elements.

4. Four-Element MIMO Antenna Configuration—Third Iteration

MIMO systems enhance channel capacity by integrating multiple antenna elements, enabling increased data transmission rates without additional power consumption or spectrum allocation. In 5G NR, where high-speed data transmission across various frequencies is crucial, a novel four-element broadband mm-wave MIMO antenna design has been developed.

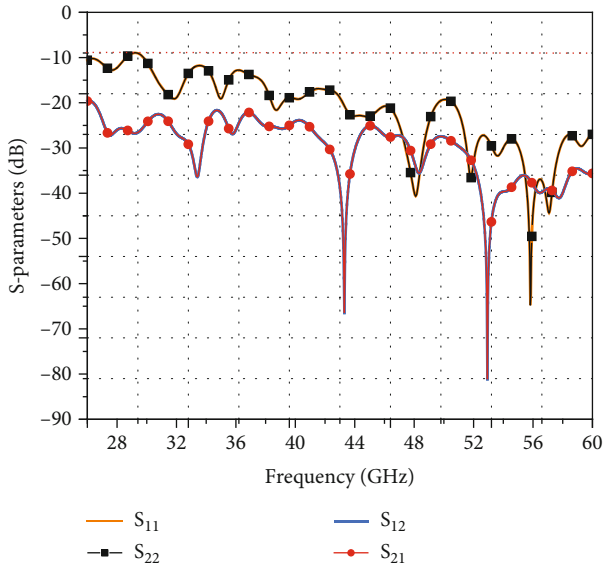

FIGURE 7: Simulated $|S_{11}|$, $|S_{22}|$, $|S_{12}|$, and $|S_{21}|$ of two-element MIMO antenna.

The MIMO antenna design, schematic diagram and perspective view, is shown in Figures 8(a) and 8(b) and is located on a Rogers RT5880 substrate measuring 25 × 26 mm^2. To improve the bandwidth, a rectangular stub measuring 5 × 4.5 mm^2 with a rectangular slot measuring 4 × 0.25 mm^2 has been introduced. There are four identical antenna elements in which two elements are arranged in a

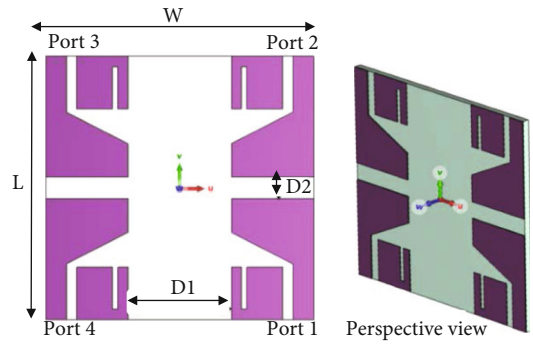

Figure 8: Schematic diagram and perspective view of the proposed four-element MIMO antenna.

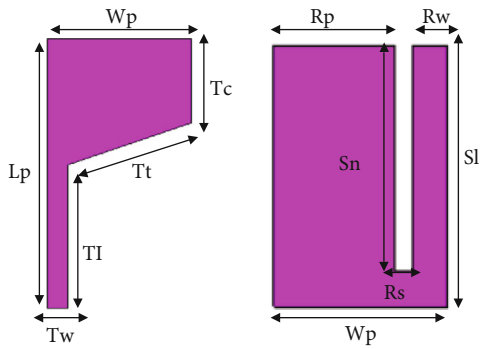

Figure 9: Geometrical representation of the proposed design.

linear configuration facing each other, while the other two are positioned in close proximity but facing opposite directions as shown in Figure 8(a). The dimensional details of the antenna are provided in Figure 9, and the top and bottom views of the fabricated antenna prototype are displayed in Figures 10(a) and 10(b), respectively.

The optimization process entails the systematic determination of the optimal interelement spacing, denoted as D1, within a range of distances to the antenna elements. The primary concern is the key performance parameters typically represented by the magnitude of the scattering parameters $|S_{11}|$ and $|S_{21}|$, as shown in Figures 11(a) and 11(b).

In particular, D1 exhibits a remarkable effect on the impedance matching characteristics of the antenna. This effect is especially pronounced when D1 is set to exactly 10 mm. This empirical observation underlines the precision with which the spacing parameter D1 can be fine-tuned to simultaneously enhance isolation, improve impedance matching, and expand the operational bandwidth of the system. Furthermore, as D1 is increased, an interesting phenomenon emerges: a substantial increase in the separation between the antenna elements becomes evident; all of this is accomplished employing any additional decoupling techniques. This observation underlines the important role of D1 in modulating and optimizing the interactions between antenna elements, especially when it is as 10 mm.

Table 1 lists the parametric values for the optimized designed antenna. By using this design, it is possible to increase the channel capacity without requiring additional power or spectrum, making it an effective solution for broadband mm-wave MIMO antenna systems used in 5G applications.

5. Results and Discussion for the Proposed Antenna Design

The obtained parameters such as reflection coefficient, transmission coefficient, gain, DG, ECC, and radiation characteristics are analyzed and explained in the following subsection.

5.1. Reflection Coefficient. Simulated reflection coefficients $|S_{11}|$, $|S_{22}|$, $|S_{33}|$, and $|S_{44}|$ are presented in Figure 12 showing similar effects in terms of bandwidth, impedance matching, and resonance. The fact that the antennas show similar reflection means that the signals transmitted from each antenna are reflected back to the receiver with similar characteristics due to the identical configuration of antenna elements.

Figure 13 demonstrates that both simulated and measured $|S_{11}|$ values cover a wide bandwidth ranging from 26 to 60 GHz. This indicates that the $|S_{11}|$ remains below -10 dB, with a VSWR of >1.8 and a fractional bandwidth (FBW) of 79.08% at the center frequency of 43 GHz, covering the entire frequency band and extending up to 60 GHz. The simulated $|S_{11}|$ plot displays a coefficient of -17.4 dB at 43 GHz center frequency, with the minimum magnitude being -35 dB at 35.4 GHz. However, upon measuring the antenna, it was discovered that the minimum coefficient of $|S_{11}|$ was -29.1 dB at 54.6 GHz and -16.3 dB at the center frequency of 43 GHz.

5.2. Transmission Coefficient. The transmission coefficients $|S_{12}|$, $|S_{21}|$, $|S_{13}|$, $|S_{31}|$, $|S_{41}|$, $|S_{14}|$, $|S_{23}|$, $|S_{32}|$, $|S_{24}|$, $|S_{42}|$, $|S_{34}|$, and $|S_{43}|$ are illustrated in Figure 14. Based on the observations, the $|S_{12}|$, $|S_{21}|$, $|S_{34}|$, and $|S_{43}|$ exhibit similar values. Additionally, these coefficients show a high level of isolation (i.e., <-25 dB), which indicates low mutual coupling between the antenna elements associated with these coefficients. Similarly, the transmission coefficients $|S_{13}|$, $|S_{31}|$, $|S_{42}|$, and $|S_{24}|$ also exhibit similar values, but with a lower level of isolation (i.e., <-19 dB). This suggests a slightly elevated mutual coupling between the antenna's

(a) (b)

Figure 10: Fabricated prototype of the proposed antenna: (a) top view and (b) bottom view.

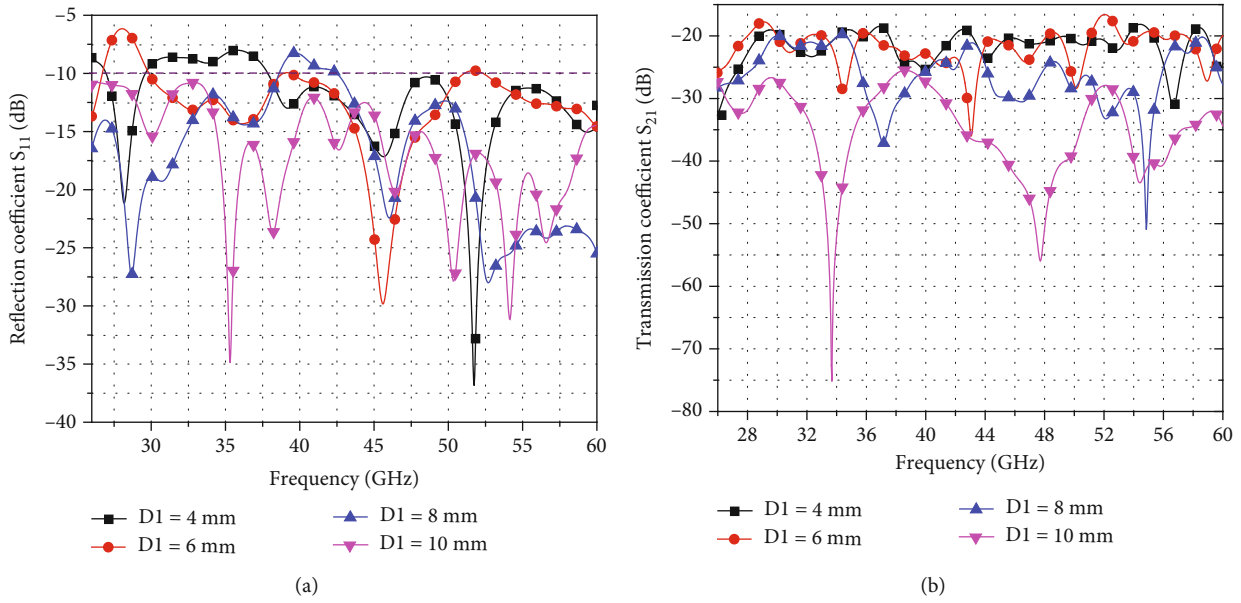

(a) (b)

Figure 11: (a) $|S_{11}|$ optimization at various distances (D1). (b) $|S_{21}|$ optimization at various distances (D1).

elements associated with these coefficients compared to the first set of coefficients, but all coefficients are within the acceptable range. Finally, the transmission coefficients $|S_{23}|$, $|S_{32}|$, $|S_{41}|$, and $|S_{14}|$ also exhibit similar values and show a high level of isolation (i.e., <-25 dB). This indicates a low mutual coupling between the antenna's elements associated with these coefficients. The antennas show better isolation in both transmission and reception due to low mutual coupling.

The simulated and measured $|S_{21}|$ are demonstrated in Figure 15. The symmetric method of a four-element antenna system is advocated to lessen mutual coupling between

Table 1: Optimized design dimensions.

Symbol	Dimensions (mm)	Symbol	Dimensions (mm)	Symbol	Dimensions (mm)
L (subs.)	25	T_t	6.71	T_w	2
W (subs.)	26	S_l	5	T_l	5.5
L_p	11.5	S_w	4.5	T_c	3
W_p	8	R_s	0.5	R_w	1
R_p	3	S_n	3.58	D1	10
D2	2				

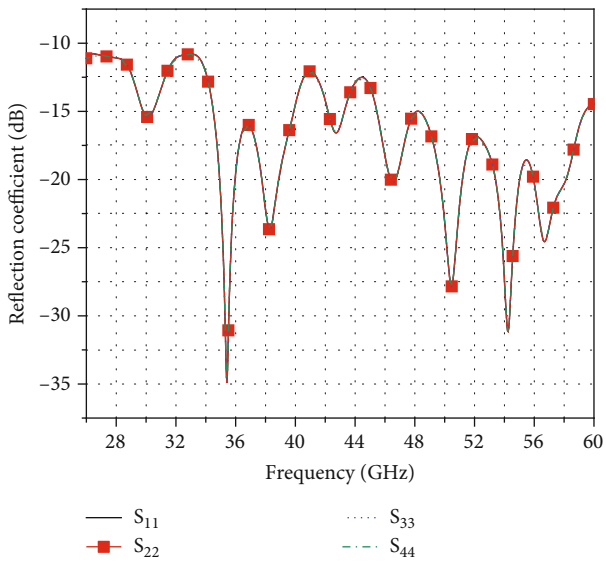

Figure 12: Simulated reflection coefficients of all ports.

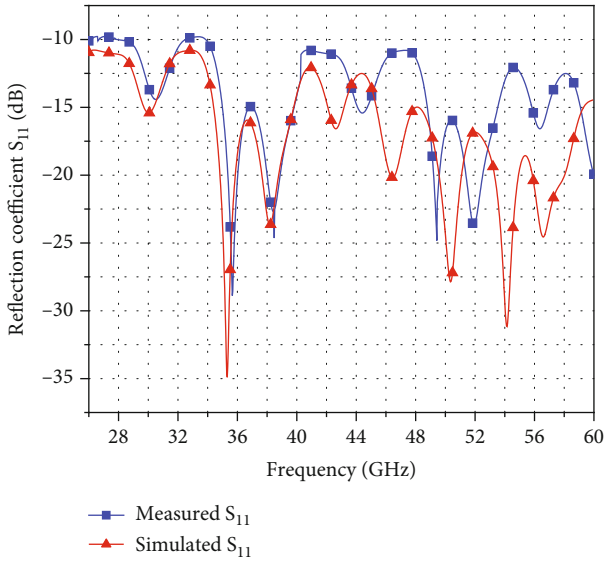

Figure 13: Simulated and measured reflection coefficient ($|S_{11}|$).

antenna ports. Due to this placement of elements with equal amplitude, isolation is very high without using any extra technique. It is observed that the simulated value $|S_{21}|$ of <-25 dB is obtained in the entire operating band. The minimum value of $|S_{21}|$ is obtained as -76.71 dB at 34.4 GHz, while in measurements, the least experimental value $|S_{21}|$ of -60 dB is achieved at 34.21 GHz. It is observed that the distance between port 1 and port 2 is quite short. The results of transmission coefficients show that the proposed antennas are highly isolated within the entire operating band. In Figure 16, both simulated and measured values of $|S_{23}|$ and $|S_{24}|$ are presented. The results indicate that the minimum value of $|S_{23}|$ is -42.2 dB, which occurs at a frequency of 38.7 GHz in the simulation.

On the other hand, the experimental data shows that the minimum value of $|S_{24}|$ is -40 dB, observed at a frequency of 38.51 GHz. For $|S_{24}|$, the simulation and measurement results show that the minimum value of $|S_{21}|$ is -52.1 dB, which occurs at 29.3 GHz in the simulation. However, the experimental data shows a lower minimum value of -60 dB, which is observed at a frequency of 34.21 GHz.

Simulation and measurement findings of S-parameters exhibit strong agreement. Insignificant variations, however, are caused by fabrication losses or the unavoidable usage of coaxial wires throughout the measurement. As a result, the measured findings show that the antenna is suitable for use in 5G applications in the future.

5.3. Current Distribution. The current distribution on each element of the MIMO antenna determines the phase and amplitude of the electromagnetic waves emanating from each element.

Figures 17(a)–17(d) illustrate the current distribution of each element of the MIMO antenna at 35.4 GHz. During the simulation, port 1 was excited while the other ports were terminated by a 50 Ω load to investigate the behavior and correlation of the antenna elements. Density meters were used to measure the current density and electric field flux within the antenna, providing a detailed visual representation. The results show that the highest current concentration is observed in the transmission line, the stub, and the edges of the patch, while the surrounding patch region exhibits the lowest current. The efficiency of an antenna is dependent on the current distribution, as it controls the antenna's ability to radiate energy effectively. Uniform current distribution in each element results in uniform radiated energy.

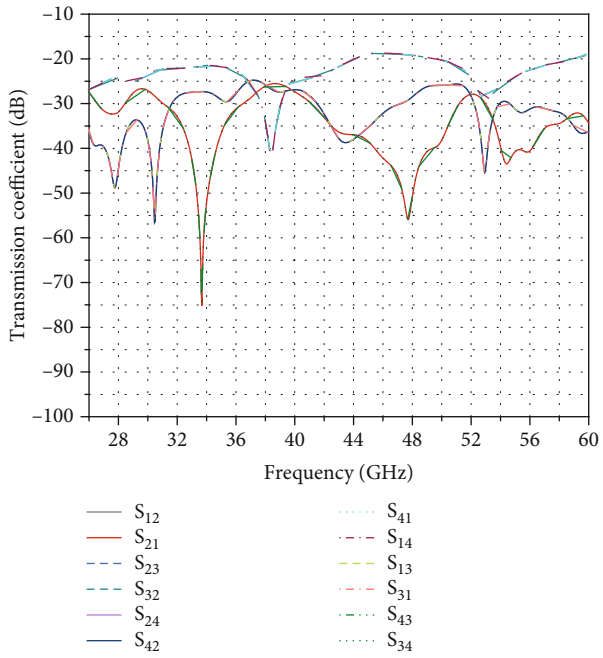

FIGURE 14: Simulated transmission coefficients of the proposed antenna.

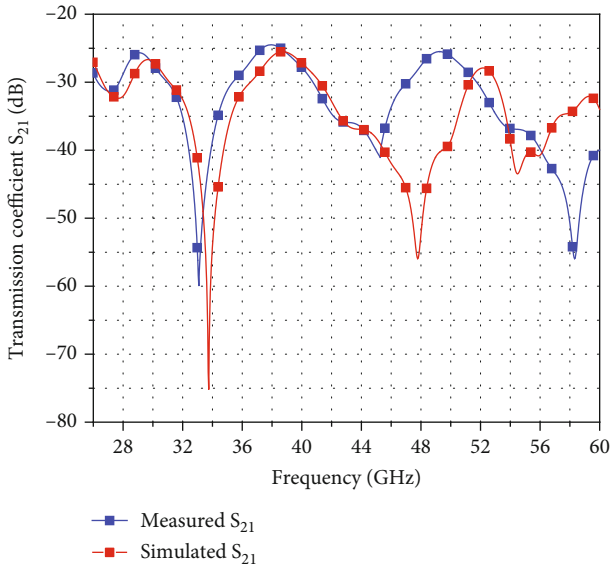

FIGURE 15: Simulated and measured $|S_{21}|$.

5.4. Gain and Radiation Efficiency. Antenna gain and radiation efficiency are crucial factors that determine an antenna's ability to transmit and receive electromagnetic waves effectively. Gain measures the antenna's radiated power in a specific direction compared to a reference antenna. Efficiency indicates how well the antenna converts input power into radiated energy. A higher efficiency means the antenna can transmit more of the input power as radiation. To measure these parameters, the antenna is placed in a controlled environment, an anechoic chamber. It is connected to a signal source or network analyzer, and a reference antenna with a known gain is positioned in the chamber as well. By comparing the received signal strength from both antennas, the gain of the antenna under test is calculated. To obtain the gain pattern, measurements are repeated for different angles or positions of the antenna. Corrections, such as cable loss or antenna factor, are applied to ensure accurate measurements. Figure 18(a) shows the simulated antenna gain performance for different phases of the design, from a single element to the final design. The single-element antenna achieves a gain of 2.9 dB, while the two-element MIMO configuration significantly improves gain to 6.4 dB. The four-element antenna design achieves a maximum gain of 11.1 dB at 60 GHz, and gain increases with frequency, indicating good broadband performance. The proposed antenna design minimizes losses in the radiation process through careful impedance matching and reduced parasitic effects. This helps in maximizing the power transfer from the transmitter to the radiating elements, leading to a higher gain. The graph confirms that using multiple antennas increases the overall gain, as they combine signals to create a stronger output compared to a single antenna. Figure 18(b) illustrates the simulated and measured gain and radiation efficiency. The experimental gain is 10.9 dB, and the radiation efficiency achieves 94%, which matches well with the simulated outcomes.

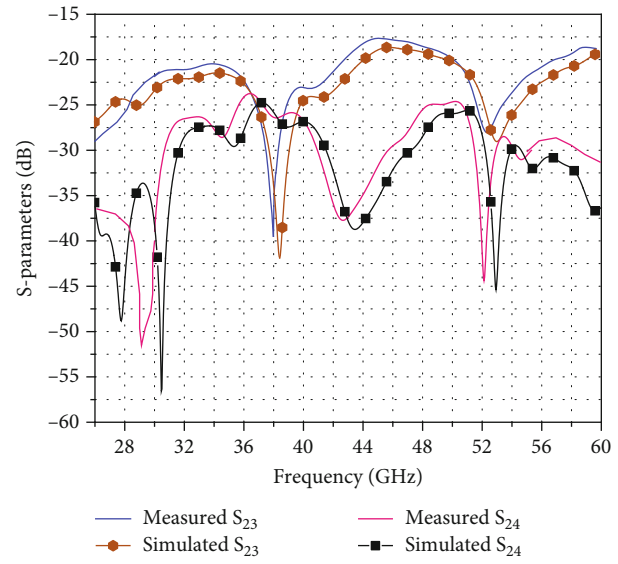

FIGURE 16: Simulated and measured $|S_{23}|$ and $|S_{24}|$.

5.5. Radiation Patterns. In this segment, the simulated and measured copolarized and cross-polarized polar patterns are demonstrated at 35.4 GHz and 54.6 GHz as displayed in Figure 19. Simulated polar graphs are obtained by using the CST tool and experimental polar graph measured inside an anechoic chamber. The measurement setup is displayed in Figure 20 for the copolarized and cross-polarized plane.

Polar patterns have radiation properties with respect to spatial coordinates phi (φ) and theta (θ) to the certain axis alignment. This includes radiation intensity, electric field or magnetic field strength, antenna directivity, and antenna's

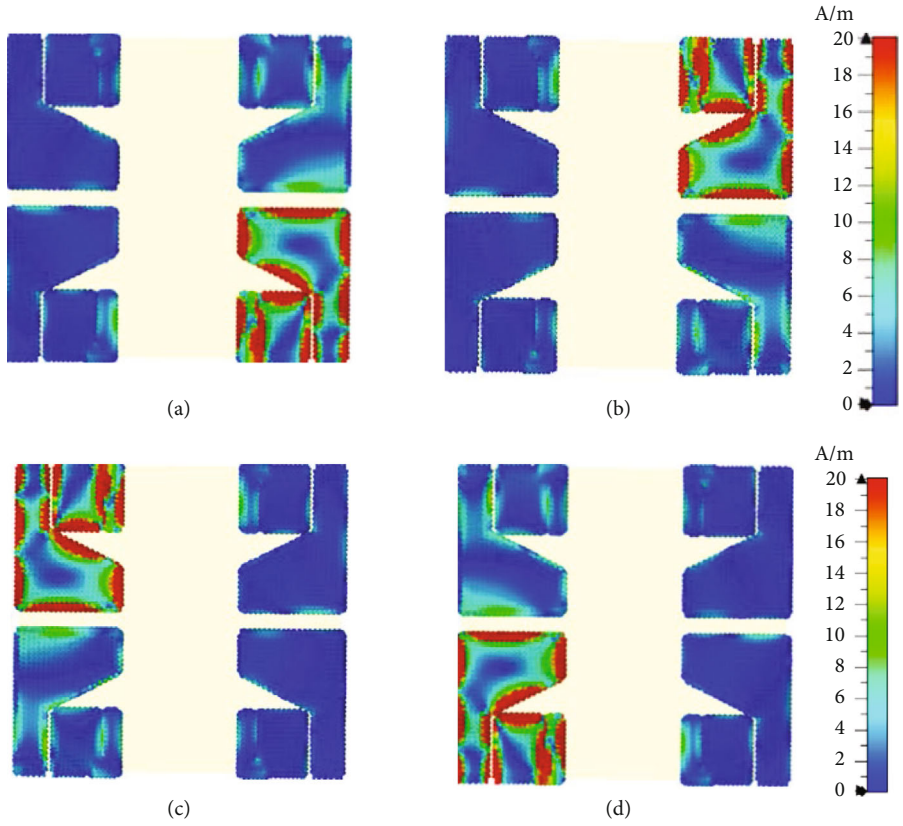

FIGURE 17: Surface current distribution at 35.4 GHz.

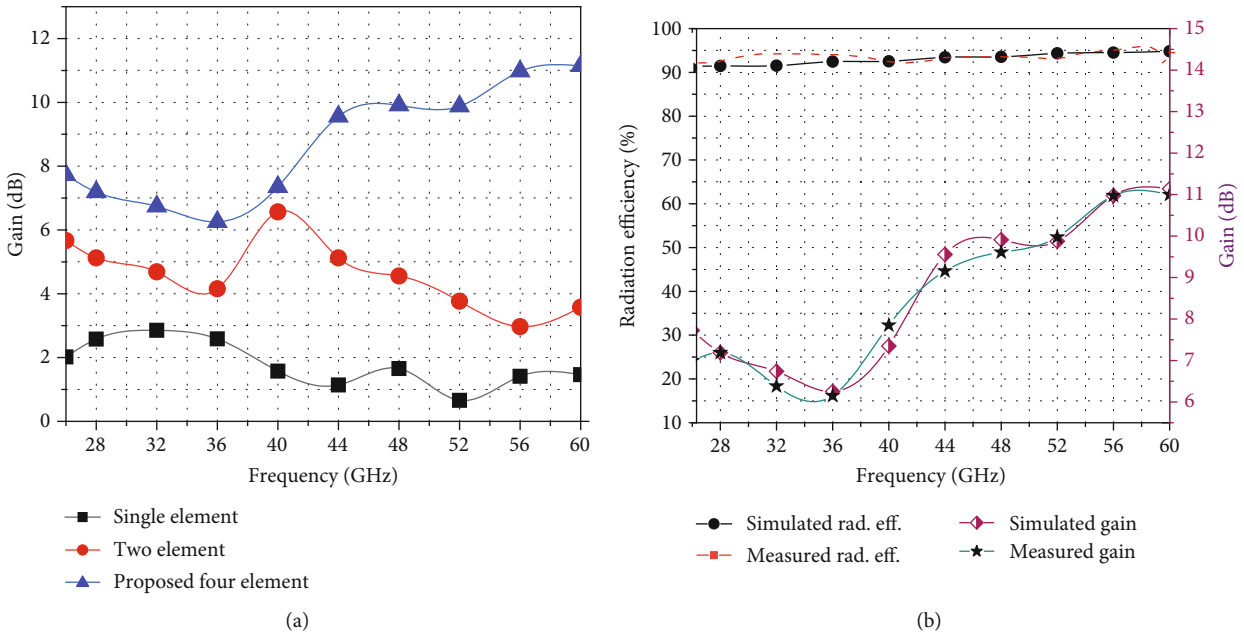

FIGURE 18: (a) Simulated gain for all three iterations. (b) Gain and radiation efficiency of the proposed antenna.

polarization properties. The simulation and measurement are carried out by exciting each port once, while the remaining three ports are connected to a matching load of 50 Ω. The 2D polar patterns are demonstrated in copolarized and cross-polarized planes when $\theta = 0^\circ$ to 360° with respect to $\varphi = 0^\circ$ (constant) and on the other hand when $\theta = 0^\circ$ to 360° when $\varphi = 90^\circ$ (constant). Simulated 2D radiation characteristics are depicted in Figure 19(a), and measured

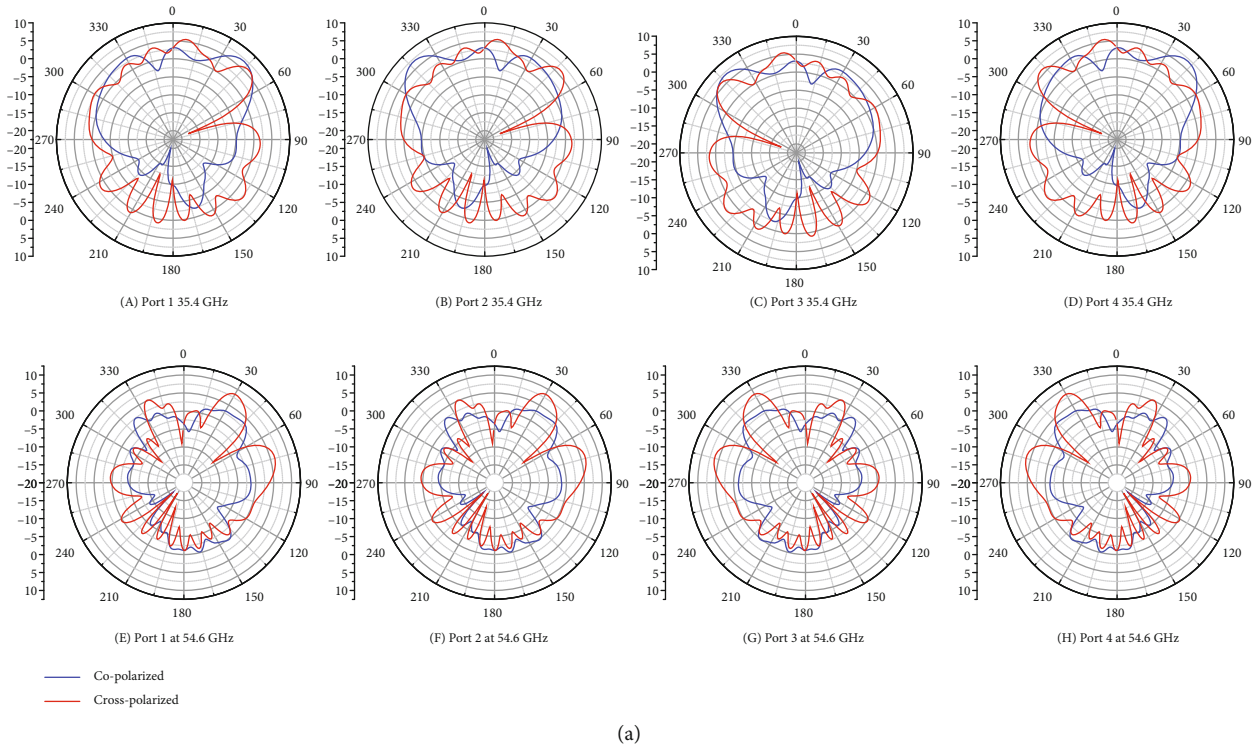

(a)

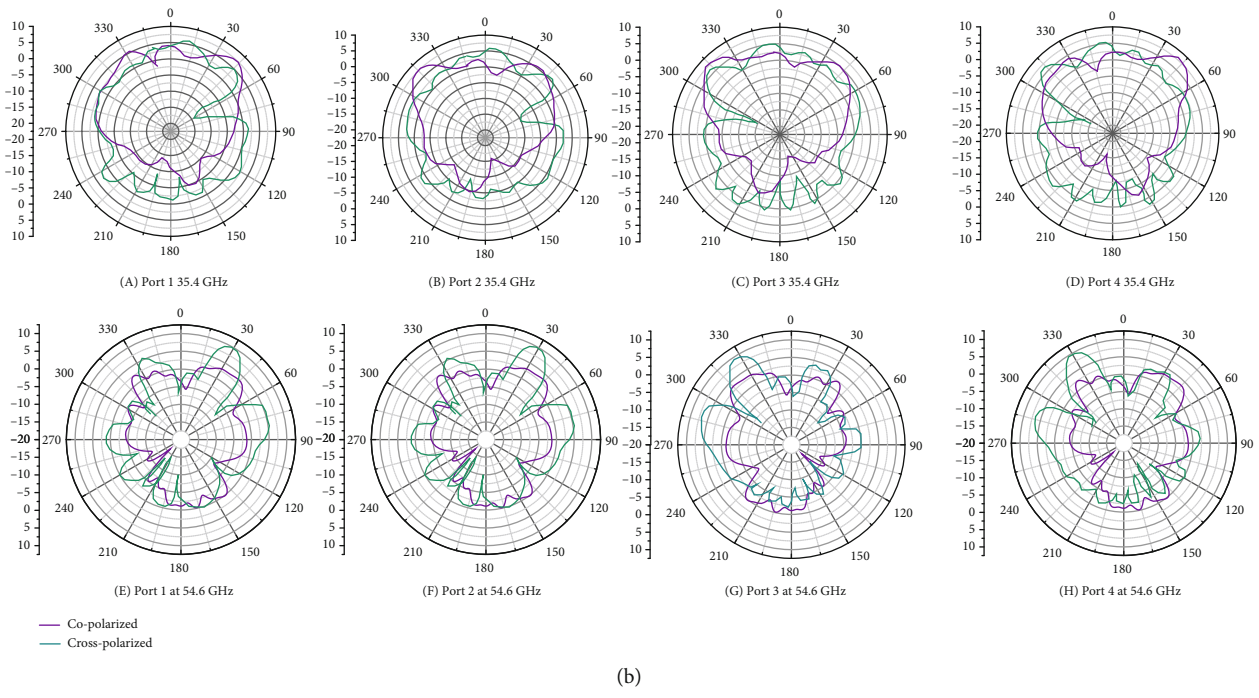

(b)

FIGURE 19: (a) Simulated 2D radiation patterns of the proposed antenna. (b) Measured 2D radiation patterns of the proposed antenna.

radiation patterns are presented in Figure 19(b) at the respective frequencies. It is important to note that the fields which emitted radiation by the antenna are almost omnidirectional. This far-field analysis demonstrates that it could be applicable to 5G technologies.

5.6. Envelope Correlation Coefficient (ECC). The ECC and DG are the important parameters to explain the diversity performance of any MIMO antenna system. The ECC is presented in Figure 21. A significant consideration to define the output of any MIMO antenna is determined by ECC [18]. It is important to conclude how the different variables of MIMO system relate to each other based on individual antenna characteristics.

The S-parameters are used to obtain the ECC analysis. ECC must be equivalent to zero, but the recommended

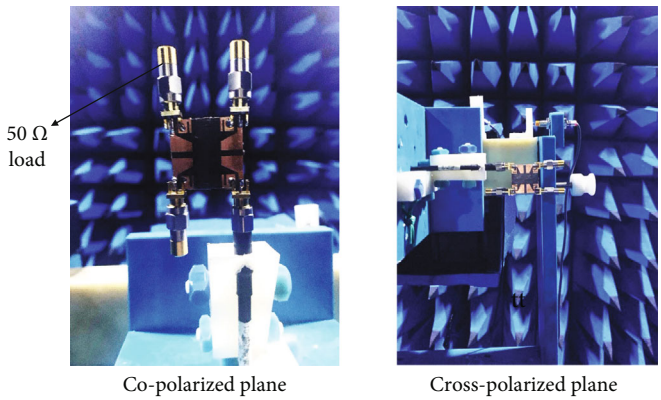

Figure 20: Measurement setup of radiation patterns inside the anechoic chamber.

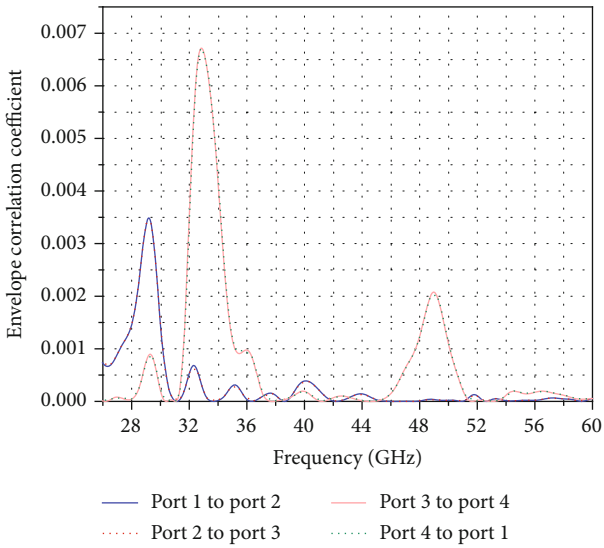

Figure 21: ECC of the proposed design.

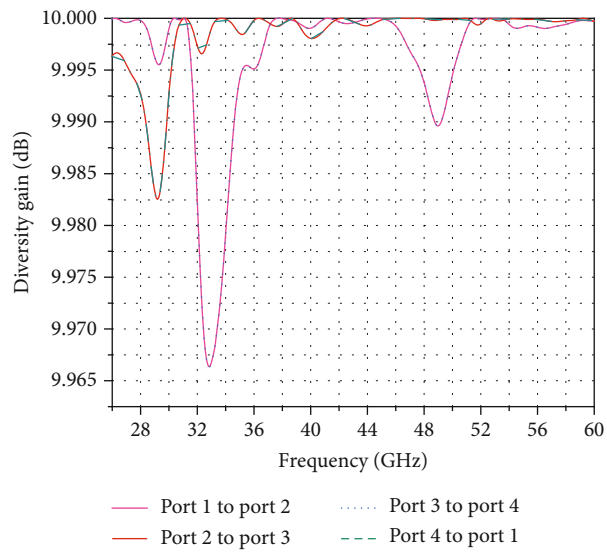

Figure 22: DG of the proposed design.

ECC must be <0.5 in MIMO antenna system. In this work, the ECC evaluation has been calculated based on simulation results.

Depending on radiation patterns, ECC is determined using equation (1). The value of ECC is obtained to be >0.00006 within the working frequency band (26-60 GHz). The low value of ECC makes this system suitable for 5G applications where high data rates are required.

$$\mathrm{ECC} = \rho_{e=} \frac{\left|\iint F_1(\theta,\varphi).\mathrm{F}_2(\theta,\varphi)|d\Omega|^2\right.}{\iint |F_1(\theta,\varphi)|^2 d\Omega \iint |F_2(\theta,\varphi)|^2 d\Omega}, \quad (1)$$

where angle (θ, φ) is the 3D radiation pattern.

5.7. Diversity Gain (DG). An essential consideration for any MIMO antenna system is the diversity gain which is also a function of ECC that can be calculated using equation (2) [19]. The DG is displayed in Figure 22. It indicates how much of the transmitted energy is reduced. The acceptable value of DG is almost 10 (9.999) dB.

$$\mathrm{DG} = 10\sqrt{1 - \mathrm{ECC}^2}. \quad (2)$$

The outcomes of single-element antenna, two-element MIMO antenna, and the proposed four-element MIMO antenna are compiled in Table 2. This comparison highlights the performance differences among the three antenna configurations, with the proposed four-element MIMO antenna demonstrating notable improvement in terms of radiation characteristics, gain, and efficiency. Table 3 provides a comparison between the proposed work and recently published literature on related antenna designs. The comparison highlights key performance metrics to evaluate the effectiveness of the proposed antenna. When comparing the proposed work with the previous studies, several notable differences emerge:

Table 2: Parameters obtained in different antenna configurations.

Parameters	Single-element antenna	Two-element MIMO antenna	Proposed four-element MIMO antenna
Impedance bandwidth	$S_{11} < -10$ dB (26-60 GHz)	$S_{11} < -10$ dB (26-60 GHz)	$S_{11} < -10$ dB (26-60 GHz)
Isolation	—	$S_{21} < -20$ dB (26-60 GHz)	$S_{21} < -25$ dB (26-60 GHz)
Gain	2.9 dB	6.4 dB	11.1 dB
Efficiency	87%	89%	94%
ECC	—	—	0.0068
Diversity gain	—	—	9.967 dB

Table 3: Comparison with the recently published literature.

Ref.	Size (mm^2)	Antenna elements	Frequency (GHz)	Bandwidth (GHz)	Isolation (dB)	Gain (dB/dBi)	ECC	DG (dB)
[20]	48×12	4	23-33 and 37.75-41	10/3.25	>20	5.7	—	>9.993
[21]	35×35	4	26.64-28.55	1.91	>27	5.07	0.0015	>9.996
[22]	47.44×32.5	4	36.83-40	3.17	>45	6.5	0.0005	>9.994
[23]	30×30	4	26-30	4	>25	7.8	0.00016	>9.985
[24]	30×30	4	26.5-29.5	3	>30	7	0.0005	>9.95
[25]	48×31	4	26-31	5	>21	6	0.0015	>9.94
[26]	12×8.5	2	27.28-28.26	1.2	>20	7 dB	0.005	>9.8
Proposed work	25×26	4	26-60	34	>25	11.1 dB	0.0068	>9.967

(i) A significantly wider frequency range of 26-60 GHz, making it suitable for a broader range of applications

(ii) Its bandwidth of 34 GHz is considerably larger than the referenced antennas

(iii) Remarkable gain performance, reaching 11.1 dB, which surpasses most of the previous works [20–27]

Some of the referenced [21, 24, 26] antennas target specific frequency bands; the proposed work offers extensive frequency coverage. This feature makes it versatile and adaptable for various applications.

6. Conclusion

A four-element mm-wave MIMO antenna has been designed and fabricated for 5G NR application. The edge-cutting technique and rectangular slot on the rectangular stub have the ability to change the properties of the designed antenna. The rotationally symmetric placement of antenna elements with equal amplitude is advantageous to increase isolation. Wider impedance bandwidth of 10 dB and more than 34 dB isolation are achieved at the antenna ports. Design provides high directivity of 10.9 dBi, almost omnidirectional patterns with the gain of 6.76 dB, and radiation efficiency of more than 91%. The observed ECC is <0.1, and diversity gain of almost 10 dB is obtained which proves the excellent diversity performance of the antenna. The simulated results have been rigorously validated through a comparison with the measured outcomes from the fabricated archetype. It is noteworthy that all simulated and measured data fall well within the permissible limits and exhibit strong coherence, affirming the reliability and accuracy of our findings. These findings demonstrate that the MIMO antenna is an exceptional option for 5G NR applications, as well as for the Ka-, Q-, and U-bands, due to its broad bandwidth and superior impedance matching.

Data Availability

The data used to support the findings of this study are included within the article.

Conflicts of Interest

The authors declare that are no conflicts of interest regarding the publication of this paper.

References

[1] M. A. Jensen and J. W. Wallace, "A review of antennas and propagation for MIMO wireless communications," *IEEE Transactions on Antennas and Propagation*, vol. 52, no. 11, pp. 2810–2824, 2004.

[2] P. Tiwari, V. Gahlaut, M. Kaushik, P. Rani, A. Shastri, and B. Singh, "Advancing 5G connectivity: a comprehensive review of MIMO antennas for 5G applications," *International Journal of Antennas and Propagation*, vol. 2023, Article ID 5906721, 19 pages, 2023.

[3] T. Deckmyn, S. Agneessens, A. C. Reniers et al., "A novel 60 GHz wideband coupled half-mode/quarter-mode substrate

integrated waveguide antenna," *IEEE Transactions on Antennas and Propagation*, vol. 65, no. 12, pp. 6915–6926, 2017.

[4] S. C. Ko and R. D. Murch, "Compact integrated diversity antenna for wireless communications," *IEEE Transactions on Antennas and Propagation*, vol. 49, no. 6, pp. 954–960, 2001.

[5] P. Rani, P. Tiwari, T. Singh, and V. Gahlaut, "A compact ground fed UWB antenna with single band notch characteristics," in *2021 2nd international conference on smart electronics and communication (ICOSEC)*, pp. 435–440, Trichy, India, 2021.

[6] P. Rani, T. Singh, and V. Gahlaut, "A comparative analysis of a CPW and partially ground fed for compact UWB antenna," in *2021 International Conference on Computer Communication and Informatics (ICCCI)*, pp. 1–6, Coimbatore, India, 2021.

[7] A. MoradiKordalivand, T. A. Rahman, and M. Khalily, "Common elements wideband MIMO antenna system for WiFi/LTE access-point applications," *IEEE Antennas and Wireless Propagation Letters*, vol. 13, pp. 1601–1604, 2014.

[8] R. Jain, P. Tiwari, A. Praveena, A. Bhardwaj, J. K. Rai, and P. Ranjan, "A novel modified P-shaped microstrip antenna for 5G mm wave applications," in *2023 First International Conference on Microwave, Antenna and Communication (MAC)*, pp. 1–4, Prayagraj, India, 2023.

[9] P. Tiwari, M. Kaushik, A. Shastri, J. K. Rai, and V. Gahlaut, "Simulated design and analysis of highly isolated 5G millimeter-waves MIMO antenna with wideband characteristic," in *2023 First International Conference on Microwave, Antenna and Communication (MAC)*, pp. 1–6, Prayagraj, India, 2023.

[10] M. S. Khan, A. D. Capobianco, M. F. Shafique, B. Ijaz, A. Naqvi, and B. D. Braaten, "Isolation enhancement of a wideband MIMO antenna using floating parasitic elements," *Microwave and Optical Technology Letters*, vol. 57, no. 7, pp. 1677–1682, 2015.

[11] M. Danneberg, N. Michailow, I. Gaspar et al., "Implementation of a 2 by 2 MIMO-GFDM transceiver for robust 5G networks," in *2015 International Symposium on Wireless Communication Systems (ISWCS)*, pp. 236–240, Brussels, Belgium, 2015.

[12] I. Shayea, T. A. Rahman, M. H. Azmi, and M. R. Islam, "Real measurement study for rain rate and rain attenuation conducted over 26 GHz microwave 5G link system in Malaysia," *IEEE Access*, vol. 6, pp. 19044–19064, 2018.

[13] N. Hussain, M. J. Jeong, J. Park, and N. Kim, "A broadband circularly polarized Fabry-Perot resonant antenna using a single-layered PRS for 5G MIMO applications," *IEEE Access*, vol. 7, pp. 42897–42907, 2019.

[14] N. Nguyen-Trong, H. H. Tran, T. K. Nguyen, and A. M. Abbosh, "A compact wideband circular polarized Fabry-Perot antenna using resonance structure of thin dielectric slabs," *IEEE Access*, vol. 6, pp. 56333–56339, 2018.

[15] P. Tiwari, M. Kaushik, A. Shastri, and V. Gahlaut, "Two element microstrip-fed slot loaded millimeter wave MIMO antenna," in *2023 International Conference for Advancement in Technology (ICONAT)*, pp. 1–5, Goa, India, 2023.

[16] H. Wong, Q. W. Lin, H. W. Lai, and X. Y. Zhang, "Substrate integrated meandering probe-fed patch antennas for wideband wireless devices," *IEEE Transactions on Components, Packaging and Manufacturing Technology*, vol. 5, no. 3, pp. 381–388, 2015.

[17] Z. Song, H. Zheng, M. Wang, E. Li, and Y. Li, "Design of one-eighth spherical dielectric resonator antenna for 5G applications," *IEEE Access*, vol. 8, pp. 9480–9487, 2020.

[18] S. Ashraf, J. A. Sheikh, U. Rasool, and Z. A. Bhat, "A low-profile high gain U slotted wide band micro-strip antenna for 5G applications," *International Journal of Electronics*, vol. 23, pp. 1–7, 2022.

[19] D. A. Sehrai, M. Asif, N. Shoaib et al., "Compact quad-element high-isolation wideband MIMO antenna for mm-wave applications," *Electronics*, vol. 10, no. 11, p. 1300, 2021.

[20] W. T. Sethi, M. A. Ashraf, A. Ragheb, A. Alasaad, and S. A. Alshebeili, "Demonstration of millimeter wave 5G setup employing high-gain Vivaldi array," *International Journal of Antennas and Propagation*, vol. 2018, Article ID 3927153, 12 pages, 2018.

[21] M. J. Jeong, N. Hussain, J. W. Park, S. G. Park, S. Y. Rhee, and N. Kim, "Millimeter-wave microstrip patch antenna using vertically coupled split ring metaplate for gain enhancement," *Microwave and Optical Technology Letters*, vol. 61, no. 10, pp. 2360–2365, 2019.

[22] M. E. Munir, S. H. Kiani, H. S. Savci et al., "A four element mm-wave MIMO antenna system with wide-band and high isolation characteristics for 5G applications," *Micromachines*, vol. 14, no. 4, p. 776, 2023.

[23] A. Sharma, A. Sarkar, M. Adhikary, A. Biswas, and M. J. Akhtar, "SIW fed MIMO DRA for future 5G applications," in *2017 IEEE International Symposium on Antennas and Propagation & USNC/URSI National Radio Science Meeting*, pp. 1763-1764, San Diego, CA, USA, 2017.

[24] M. M. Kamal, S. Yang, X. C. Ren et al., "Infinity shell shaped MIMO antenna array for mm-wave 5G applications," *Electronics*, vol. 10, no. 2, p. 165, 2021.

[25] S. Rahman, X. C. Ren, A. Altaf et al., "Nature inspired MIMO antenna system for future mmWave technologies," *Micromachines*, vol. 11, no. 12, p. 1083, 2020.

[26] S. Kumar, N. N. Tiwari, A. Mohammed Arif, A. K. Dwivedi, and V. Singh, "MIMO antenna with low mutual coupling and high gain for n257-band 5G mm-wave," in *2023 13th International Symposium on Advanced Topics in Electrical Engineering (ATEE)*, pp. 1–5, Bucharest, Romania, 2023.